Aalborg Universitet

Event-triggered hybrid control based on multi-Agent systems for Microgrids

Dou, Chun-xia; Liu, Bin; Guerrero, Josep M.

Event-triggered hybrid control based on multi-agent system for Microgrids

Chun-xia Dou[*,1], Bin Liu[2], Josep M. Guerrero[3],

*1.   Institute of Electrical Engineering, Yanshan University, Qinhuangdao 066004, P.R. China.

(e-mail: cxdou@ysu.edu.cn)

2. The University of Sydney, NSW 2006, Australia and Department of Information and Computation Sciences, Hunan University of Technology, Zhuzhou 412008, P.R. China.

(e-mail: bin.liu@sydney.edu.au)

3. Department of Energy Technology, Aalborg University, 9220 Aalborg East, Denmark

(e-mail:joz@et.aau.dk)

Abstract—This paper is focused on a multi-agent system based event-triggered hybrid control for intelligently restructuring the operating mode of an microgrid (MG) to ensure the energy supply with high security, stability and cost effectiveness. Due to the microgrid is composed of different types of distributed energy resources, thus it is typical hybrid dynamic network. Considering the complex hybrid behaviors, a hierarchical decentralized coordinated control scheme is firstly constructed based on multi-agent system, then, the hybrid model of the microgrid is built by using differential hybrid Petri nets. Based on the hybrid models, an event-triggered hybrid control including three kinds of switching controls is constructed by designing multiple enabling functions that can be activated by different triggering conditions, and the interactive coordination among different switching controls is implemented through the intelligent multiple-agent system platform, so that the operating mode of MG can be intelligently restructured in flexible manner according to the changes of operating situation. The validity of proposed control scheme is demonstrated by means of simulation results.

Index terms—**Microgrid, event-triggered hybrid control, multi-agent system, switching control, distributed energy resource**

1   Introduction

Global problems like the growing demand on energy, shortage of energy supply, and environment concerns, have motivated the exploitation and utilization of clean and renewable energy sources. The increasing penetration of Distributed Energy Resources (DERs) in recent power network brought the new concept Microgrid (MG) [1,2]. The MG which is formed generally by confined cluster of loads, storage devices, and small generators also named as microsources, has received increasing attention as an effective way of integrating DERs into the electricity network. The MG has the ability as single entity to work in both grid-connected and islanded modes of operation [3-5]. So far, in a MG, control system is ordinarily composed by an energy management system for whole MG and many local continuous dynamic controls for each component unit, where there is rarely intelligent switching control for operating mode. In order to ensure that the MG can effectively use DERs to provide continuous power supply with high reliability, stability and cost effectiveness, the intelligent switching control strategies for operating mode need be constructed [6-8]. However, designing the intelligent switching control, there are many challenging problems as follows:

1) Complex component and structure; a MG contains many kinds of DERs, divided into Distributed Generation Units (DGUs) and distributed storage devices, and displaying different behavior characteristics. Moreover, many DER units are non-50/60Hz, must using power-electronic converter interfaces when they are connected into network. All the above factors lead to that the component and structure of a MG is very complex [9,10].

2) Complex hybrid dynamic behaviors; in a MG, many DERs display both continuous and discrete dynamic behaviors. In detail, their generation electricity characteristics show continuous dynamic behaviors. Simultaneously, they have to be frequently switched between different operating modes due to environment condition or load changes, which are described as event-driven discrete behaviors. Moreover, these hybrid behaviors interact tightly with each other [11-15].

3) Uncertain operation situation; in a MG, the power outputs of many renewable energy resources highly depend on natural energy conditions. As a result, such resources often provide intermittent and uncertain energy supply. Moreover, a MG usually provides services to end users whose power demands are also variable and unpredictable. In addition, some DER units need operate in "plug-and-play" manner. All the above factors imply that the MG usually operates in an uncertain environment.

With respect to above the challenging problems, when design the intelligent switching control strategies, it is necessary to consider the following means:

1) The control scheme should be constructed as a hierarchical Multi-Agent System (MAS) so as to intelligently reconstruct the operating mode against uncertain environment.

The MAS should be composed of different agents associated with different DER units, and any one of them is capable to respond adequately to operation situation via switching operating mode by their reactive layer. They also have high intelligence to control or plan the behaviors of the own agent according to the change of environment, so as to achieve their intentions by means of the deliberative layer [16,17]. Moreover, the different hierarchical agents can negotiate and interact to restructure the operating mode of the MG in cooperative manner so as to make whole system adapt uncertain environment [18,19].

2) The switching control strategies should be designed as event-triggered hybrid controls including continuous dynamic triggering, discrete event triggering as well as their interactions so as to effectively control the complex hybrid behaviors.

Corresponding to the complex hybrid behaviors of the MG, the switching control for operating mode not only can be driven by continuous dynamic behaviors, but also can be triggered by discrete-event behaviors, even more important, the different kinds of switching controls should tightly coordinate and timely interact with each other according to the hybrid characteristic. In this case, the switching control is called as event-triggered hybrid control [20-22].

For the reasons given above, in this paper, we propose a MAS based event-triggered hybrid control in order to for the purpose of higher security, stability and cost effectiveness.

Firstly, a hierarchical decentralized coordinated control scheme is constructed based on MAS platform. Then the hybrid

model of the MG is built by using Differential Hybrid Petri-net (DHPN). As an original research, based on the DHFN model, an event-triggered hybrid control is constructed, consisted of three kinds of switching controls: (1) internal switching control for operating mode driven by the constraint conditions of local continuous state variable, which is implemented in every unit agent, (2) global coordinated switching control for operating mode among unit agents triggered by Voltage Security Assessment Index (VSAI), which is constituted in the upper level agent, and (3) switching control for continuous dynamics triggered by the change of operating mode, which is also implemented in every unit agent. And the three kinds of switching controls are designed via different enabling functions associated with arcs based on DHPN models respectively, and interactive coordination among them is implemented on intelligent MAS platform, so that the operating mode of MG can be intelligently restructured in flexible manner.

The paper is organized as follows. The MAS based control scheme is constructed in Section 2. In Section 3, the MG hybrid model is built by using DHPN. The event-triggered hybrid control is researched in Section 4. The experiment study is presented in Section 5. Concluding remarks are summarized in Section 6.

2   MAS based decentralized coordinated control scheme

In this paper, an example of autonomous MG is shown in Fig.1, which contains a photovoltaic energy generation unit, a wind energy generation unit, a fuel cell and microturbine generation unit, a battery unit and a group of loads. A MAS based two level control scheme is here proposed, that is, internal switching controls for each DER unit are carried out by the lower level unit agent, and the coordinated switching controls for operational mode are implemented through the upper level coordinated control agent. The function structure of the hierarchical MAS is designed as Fig.2.
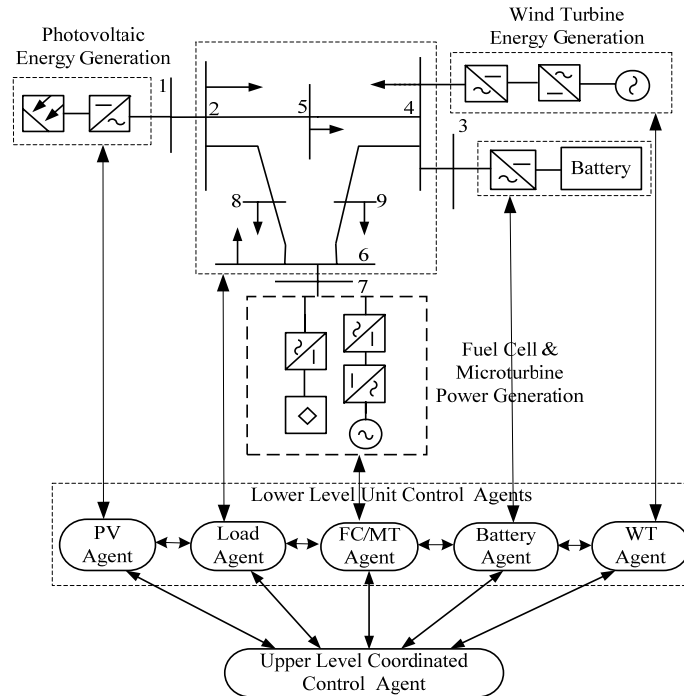

Fig.1. MAS based control scheme of an autonomous MG

In Fig.2, the lower level unit agent is designed as a hybrid agent, consisted of reactive layer and deliberative layer. The reactive layer that is defined as "recognition, perception and action", has priority to quickly respond to emergencies of the environment. For instance, the reactive layer of the wind energy generation unit agent can perceive a sudden change of wind speed so as to determine whether to switch its operating mode. The deliberative layer that is defined as "belief, desire and intention", has higher intelligence to control or plan agent behaviors via the local control strategies so as to achieve its intention. And the local control strategies are constituted based on knowledge data and state evaluation and are implemented through the action module.

The upper level coordinated control agent is designed as a deliberative agent. Its intention is to coordinately control the operating modes so as to ensure the energy supply with high reliability and high benefit. The coordinated switching control is established in the decision-making module by using the VSAI, and is implemented through the action implementation module. The VSAI is evaluated in the security assessment module based on knowledge data and data base.
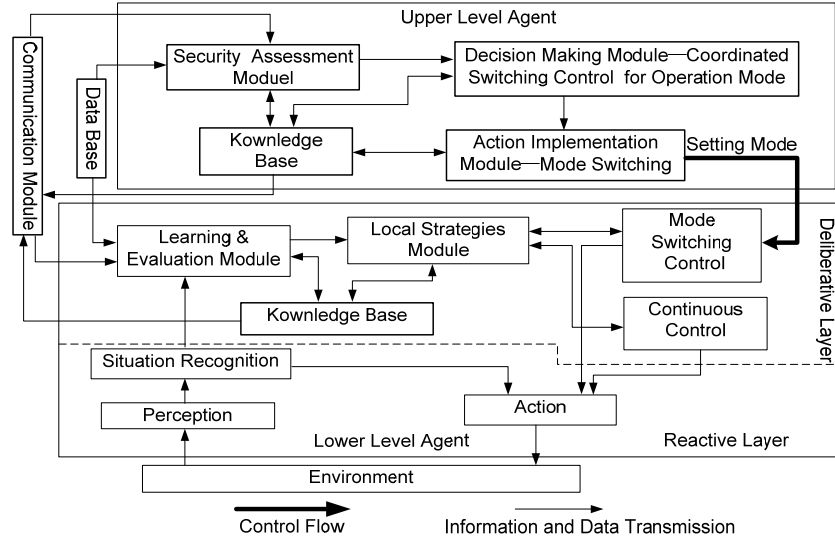
Fig.2. Structure of MAS based decentralized coordinated control

3   MAS Based hybrid model

3.1 Differential Hybrid Petri-net

In this section, for the purpose of designing the event-triggered hybrid control, a MAS based DHPN model is firstly built to describe hybrid behaviors of the MG. The description regarding the DHPN is give as follows:

A DHPN can be defined by a 14-tuple (P_D, T_D, P_{DF},T_{DF}, X , A_N, A_I, A_T, P_{re}, P_{os}, Γ , H, J, M_0) [23-25], where

$P_D =\{P_1,P_2,\ldots,P_v\}$ is a finite and nonempty set of discrete places. $P_i \in P_D$ describes the discrete state of the hybrid system;

$T_D =\{T_1,T_2,\ldots,T_w\}$ is a finite and nonempty set of discrete transitions. $T_i \in T_D$ describes the occurrence of discrete events in the hybrid system;

$P_{DF} =\{P_{1f},P_{2f},\ldots,P_{rf}\}$ is a finite and nonempty set of differential places. $P_{if} \in P_{DF}$ describes the continuous state;

$T_{DF} = \{T_{1f}, T_{2f}, \ldots, T_{qf}\}$ is a finite and nonempty set of differential transitions. $T_{if} \in T_{DF}$ describes the continuous dynamics;

$X = [x_1, x_2, \cdots x_n]^T$ is a continuous state vector related with a differential place $P_{if} \in P_{DF}$. $X_0 = [x_{10}, x_{20}, \cdots x_{n0}]^T$ is the initial continuous state vector of the hybrid system;

$P = P_D \cup P_{DF}$, $T = T_D \cup T_{DF}$, $P \cap T = \phi$, $P \cup T \neq \phi$;

$A_N \subseteq ((P_D \times T_D) \cup (T_D \times P_D)) \cup ((P_D \times T_{DF}) \cup (T_{DF} \times P_D))$, is a set of normal arcs;

$A_I \subseteq (P_D \times T_D)$, is a set of inhibitor arcs;

$A_T \subseteq (P_{DF} \times T_D) \cup (T_D \times P_{DF})$, is a set of test arcs;

P_{re} defines a predecessor incidence divided into three kinds: $P_{reD}(P_i, T_j)$ is a function that defines the normal arcs from a discrete place ($P_i \in P_D$) to a discrete transition ($T_j \in T_D$); $P_{reDDF}(P_i, T_{jf})$ is a function that defines the normal arcs from a discrete place ($P_i \in P_D$) to a differential transition ($T_{jf} \in T_{DF}$); $P_{reDI}(P_i, T_j)$ is a function that defines the inhibitor arcs from a discrete place ($P_i \in P_D$) to a discrete transition ($T_j \in T_D$); and the values of these functions are positive integer;

P_{os} defines a posterior incidence divided into three kinds: $P_{osD}(P_i, T_j)$ is a function that defines the normal arcs from a discrete transition ($T_j \in T_D$) to a discrete place ($P_i \in P_D$); $P_{osDDF}(P_i, T_{jf})$ is a function that defines the normal arcs from a differential transition ($T_{jf} \in T_{DF}$) to a discrete place ($P_i \in P_D$); $P_{osDFF}(P_{if}, T_{jf})$ is a function that defines the normal arcs from a differential transition ($T_{jf} \in T_{DF}$) to a differential place ($P_{if} \in P_{DF}$); and the values of the front two kinds of functions are positive integers;

Γ is a timing map for the discrete transitions, that is $\Gamma(T_j) = d_j \in R \geq 0$;

$H_{DF}(P_{if}, T_j)$ is defined as an enabling function associated with a test arc that connects a differential pre-place to a discrete transition. By the enabling function, the triggering condition of the discrete transition can be defined according to the continuous state variables;

$H_D(P_i, T_j)$ is defined as an enabling function associated with a arc that connects a discrete pre-place to a discrete transition. It implies that the triggering condition of the discrete transition depends on the enabling function;

$J(T_j, P_{if})$ is a junction function associated with a test arc that connects a discrete transition to a differential post-place;

M_0 is the initial marking of places in t=0. Corresponding to a discrete (differential) place, its marking and the initial marking are represented by $m_D(P_i)$ ($m_F(P_{if})$) and $m_{D0}(P_i)$ ($m_{F0}(P_{if})$) respectively.

3.2 MAS Based DHPN Model

Corresponding to the six agents as shown in Fig.1, the hybrid model of the MG is described by integrating six DHPN models as shown in Fig.3, including one coordinated control DHPN model and five unit control DHPN models. More detailed descriptions regarding the places and the transitions are given in Tables 1-4 in the Appendix.

Where all discrete transitions are defined as "logically true", That is, a discrete transition is triggered when its connected enabling function is activated. At the moment, only if the pre-place has token, then the corresponding mode switching must occur, known as "transition fires".

Where all differential transitions $T_{1f} - T_{9f}$ can be described by the differential equation $\dot{\mathbf{x}}_i = f_{is}(\mathbf{x}_i, \mathbf{u}_{is}, t)$, where, i represents the i-th agent, and s is the s-th mode of the i-th agent.

Normal arc functions $P_{reD}(P_i, T_j)$, $P_{reDDF}(P_i, T_{jf})$, $P_{osD}(P_i, T_j)$ and $P_{osDDF}(P_i, T_{jf})$ mentioned in subsection A are defined as "1". In addition, the normal arc functions $P_{osDFF}(P_{if}, T_{jf})$ is denoted as the continuous state vector of the i-th agent.
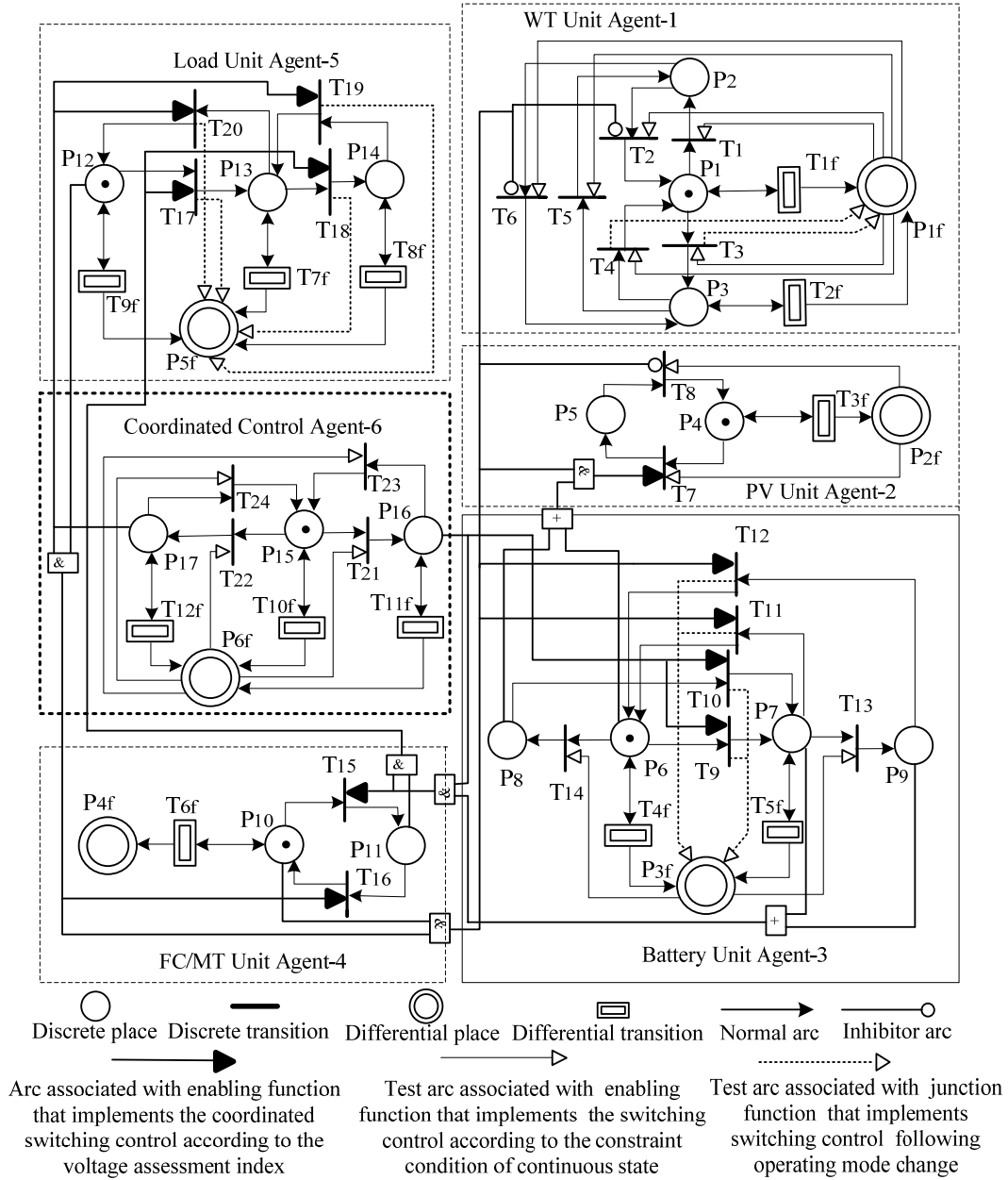

Fig.3. MAS based event-triggered hybrid control on the DHPN model

Since each agent can only run in one mode, and the corresponding place is marked with a token, while other places

have not token. Therefore, there is only one token in each agent DHPN model. When the operating mode is switched, the token is transformed into corresponding post-place from the pre-place. In the DHPN model, corresponding to the initial modes of six agents, the initial marking are respectively: $m_{D10}(P_i)=[1,0,0]$, $m_{D20}(P_i)=[1,0]$, $m_{D30}(P_i)=[1,0,0,0]$, $m_{D40}(P_i)=[1,0]$, $m_{D50}(P_i)=[1,0,0]$, $m_{D60}(P_i)=[1,0,0]$; and $m_{F10\text{-}F60}(P_{if})$ are the initial state vectors $\mathbf{x}_{i0}$ of the six agents respectively.

By the above description, the DHPN model shows only hybrid dynamic behavior of the MG, but no hybrid switching control is taken. For the purpose of security, stability and high efficiency, a MAS based event-triggered hybrid control is here designed including three kinds of switching controls: (1) internal switching control for operating mode according to constraint conditions of local continuous state variable in every unit agent, (2) global coordinated switching control for operating mode among unit agents based on voltage stability assessment, and (3) switching control for continuous dynamics in every unit agent following the change of operating mode. As a very creative idea, here, based on the DHPN model, these hybrid control actions are implemented via enabling functions and junction functions associated with test arcs, normal arcs and inhibitor arcs. Therefore, how to design these arc functions is a very important issue. More detail designs regarding three kinds of switching controls will be discussed in the following section.

4   MAS based event-triggered hybrid control

4.1 Design of the Switching Control Based on the Constraints of Continuous State Variables

According to the constraint conditions of the continuous state variable, the switching control for operating mode is constituted in the local strategy module in respective lower level unit agent and is designed by means of the enabling function H_{DF} (P_{if},T_j) for the purposes regarding cost effectiveness and system protection. The switching control has the following features: (1) it is a discrete control driven by continuous state variables (2) it is triggered to switch operating mode when the constraint conditions of the continuous state are violated, and (3) it executes mode switching within unit agent according to its local continuous states. In Fig. 3, the switching control via H_{DF} (P_{if},T_j) is design as follows

$$H_{DF}(P_{1f},T_1) \xrightarrow{\downarrow} v \le v_{ci} \Rightarrow P_w = 0 \,; \tag{1}$$

$$H_{DF}(P_{1f},T_2) \xrightarrow{\uparrow} v_{ci} < v \le v_R \Rightarrow P_w = P_R(v-v_{ci})/(v_R-v_{ci})\,; \tag{2}$$

$$H_{DF}\ (P_{1f},T_3) \xrightarrow{\uparrow} v_R < v \le v_{co} \Rightarrow P_w = P_R\,; \tag{3}$$

$$H_{DF}\ (P_{1f},T_5) \xrightarrow{\uparrow} v > v_{co} \Rightarrow P_w = 0\,; \tag{4}$$

$$H_{DF}\ (P_{1f},T_6) \xrightarrow{\downarrow} v_R < v \le v_{co} \Rightarrow P_w = P_R\,; \tag{5}$$

$$H_{DF}\ (P_{1f},T_4) \xrightarrow{\downarrow} v_{ci} < v \le v_R \Rightarrow P_w = P_R(v-v_{ci})/(v_R-v_{ci})\,; \tag{6}$$

where P_R is the rated power of the wind turbine; v_{ci} is the cut-in wind speed; v_{co} is the cut-off wind speed; v_R is the rated wind speed; "$\downarrow$" represents that the wind speed drops, and "$\uparrow$" represents that the wind speed rises. The following descriptions are in the same manner.

$$H_{DF}\ (P_{2f}, T_7) \xrightarrow{\downarrow} G_{ing} \leq C \Rightarrow P_{PV} = 0\ ; \tag{7}$$

$$H_{DF}\ (P_{2f}, T_8) \xrightarrow{\uparrow} G_{ing} > C \Rightarrow P_{PV} = P_{stc} \frac{G_{ing}}{G_{stc}} \left(1 + k\left(T_c - T_r\right)\right)\ ; \tag{8}$$

where P_{PV} is the PV output power at irradiance G_{ing} ; P_{stc} is the maximum power at the standard condition; G_{ing} is the incident irradiance; G_{stc} is the standard irradiance of 1000W/m^2 ; k is the temperature coefficient; T_c is the cell temperature; T_r is the reference temperature 25 $^\circ$C, and C is the threshold G_{ing} value according to the performance of the PV cell.

$$H_{DF}\ (P_{3f}, T_{13}) \xrightarrow{\downarrow} SOC = SOC_{min} \Rightarrow P_{-} = 0\ ; \tag{9}$$

$$H_{DF}\ (P_{3f}, T_{14}) \xrightarrow{\uparrow} SOC = SOC_{max} \Rightarrow P_{+} = 0\ ; \tag{10}$$

where P_{+} and P_{-} are the charge and the discharge power of battery respectively; SOC_{max} and SOC_{min} are the maximum and the minimum state of charge (SOC).

$$H_{DF}\ (P_{6f}, T_{21}) \xrightarrow{\downarrow} m(U) \leq U_{min}; \tag{11}$$

$$H_{DF}\ (P_{6f}, T_{22}) \xrightarrow{\uparrow} m(U) \geq U_{max}; \tag{12}$$

$$H_{DF}\ (P_{6f}, T_{23}) \xrightarrow{\uparrow} U_{min} < m(U) \leq U_e; \tag{13}$$

$$H_{DF}\ (P_{6f}, T_{24}) \xrightarrow{\downarrow} U_e < m(U) < U_{max}; \tag{14}$$

where $m(U)$ is the VSAI; U_{min} is the minimal secure threshold value of voltage; U_e is the rated voltage; U_{max} is the maximal secure threshold value of voltage. The VSAI is determined by information fusion technique of voltages in many nodes, which will be addressed in detail in the following subsection.

Through all the above enabling function $H_{DF}\ (P_{if}, T_j)$ designed in (1)-(14), the switching control for operating mode within every unit agent is constructed as "$\longrightarrow\!\!\triangleright$" in Fig.3, and its implementing is described in Table 5 in the Appendix.

The above design implies that when the constraint condition of the continuous state is violated, the corresponding enabling function is activated, so that the connected transition is triggered to switch the operating mode. The switching control achieves intelligent restructure of operating mode according to constrain conditions of local continuous states in every the agent.

4.2 Voltage Security Assessment Index

The switching control for the operating mode in the coordinated control agent#6 as shown in Fig.3 need be designed based on the indicator of voltage security. In power systems, an insecure voltage generally manifests as a slow initial decay followed

by a sharp decline at the point of collapse, thus the voltage magnitude by itself is not a reliable indicator of security, and using a threshold value on the voltage magnitude to evaluate security may lead to wrong conclusions [26]. Therefore, in this paper, a more reliable VSAI is discussed in detail as follows.

4.2.1 Feature Parameters Regarding Voltage Security

The voltage sequences from the 1-st to the 9-th bus as shown in Fig.1, measured at the rate of 30 frames/s, are represented as $V_i = [V_i^1, V_i^2, ..., V_i^N]$, $i \in 1,2,\cdots,9$. Based on the voltage sequences, the feature parameters regarding voltage security are extracted by following steps

(1) the moving average value of the i-th bus voltage at the j-th instant from N available measurements is obtained as

$$V_i^{(j)} = \sum_{k=1}^{j} V_i^k \Big/ j \quad j \in 1,2,\cdots,N; \quad if \ j \le N; \qquad V_i^{(j)} = \sum_{k=j-N+1}^{j} V_i^k \Big/ N \quad j \in N+1, N+2,\cdots,m; \quad if \ j > N ; \qquad (15)$$

(2) the percentage of diversity between the measured voltage $V_i^{\ j}$ and moving average value $V_i^{(j)}$ at the j-th instant is defined as

$$C_i^j = \frac{V_i^{\ j} - V_i^{(j)}}{V_i^{(j)}} \times 100, \ j \in 1,2,\cdots,m ; \qquad (16)$$

(3) the feature parameter value regarding voltage security at the j-th instant is extracted by dividing the area under the percentage of diversity curve

$$U_i^{(j)} = \sum_{k=1}^{j} (C_i^k + C_i^{k-1}) \Big/ 2j \quad j \in 1,2,\cdots,N; \quad if \ j \le N;$$

$$U_i^{(j)} = \sum_{k=j-N+1}^{j} (C_i^k + C_i^{k-1}) \Big/ 2N, \qquad j \in N+1, N+2,\cdots,m; \quad if \ j > N. \qquad (17)$$

Through the above transform, the feature parameter sequences corresponding to the 1-st to the 9-th bus are obtained respectively, which can reliably predict the voltage security of each bus.

4.2.2 VSAI Based on Information Fusion Technique of Dempster-Shafer (D-S) Evidence Theory

In order to estimate the security of the whole MG, the above feature parameter sequences of all buses must be effectively integrated as a comprehensive indicator. Therefore, an information fusion technique based on D-S evidence theory is here proposed.

Firstly, based on the feature parameter sequences, a set of basic probability function is constructed as

$$m_i^j(U) = U_i^{(j)} \Big/ [U_i^{(j)} + (1-\gamma_i)] ; \quad i \in 1,2,\cdots,9 , \quad j \in 1,2,\cdots,m ; \qquad (18)$$

where $m_i^j(U)$ denotes basic probability assignment of feature parameter on the i-th bus at the j-th instant; γ_i is the weight coefficient of voltage on the i-th bus, which is limited to rational numbers between 0 and 1.

According to the D-S evidence theory [27], the fusion criterion of two different basic probability functions is

$$m(c) = \begin{cases} 0 & c = \Phi \\ K^{-1} \sum_{A_i \cap B_j = c} m_1(A_i) m_2(B_j) & c \neq \Phi \end{cases} \quad ; \tag{19}$$

$$K = 1 - \sum_{A_i \cap B_j = \Phi} m_1(A_i) m_2(B_j) \cdot \tag{20}$$

In light of (19) and (20), the $m_i^j(U)$ at different instants $j \in \{1,2,\cdots m\}$ are fused one by one, whose result is defined as $m_i(U)$.

Then, the $m_i(U)$ on different buses $i \in \{1,2,\cdots,9\}$ are fused again one by one, whose outcome is defined as the VSAI. The VSAI is

usually limited to the rational number between 0 and 1.

4.3 Design of the Coordinated Switching Control for Operating Mode Based on the VSAI

The coordinated switching control for operating mode, whose intention is to ensure system high security and low operating

cost, is designed in the decision making module at the upper level agent, and is implemented via the enabling function H$_D$

(P$_i$,T$_j$). The switching control presents the following features: (1) it is a discrete control driven by the VSAI, (2) it is triggered

to switch operating mode when the voltage is judged insecure by the VSAI, and (3) it implements the mode coordinated

switching among agents. In addition, the inhibitor function P$_{reDI}$(P$_i$, T$_j$) is designed to restrict some mode switching under cer-

tain conditions. In order to establish the coordinated switching control, logic relationships of the operating modes among unit

agents are set by using logic circuits as follows

$$\overline{P} = P_{16} \ (P_7 + P_9); \tag{21}$$

$$\overline{\overline{P}} = P_{11}P_{16} \ (P_7 + P_9); \tag{22}$$

$$\widetilde{P} = P_{12}P_{17}; \tag{23}$$

$$\widetilde{\widetilde{P}} = P_{10}P_{12}P_{17}; \tag{24}$$

$$\hat{P} = P_{10}P_{12}P_{17} \ (P_6 + P_8). \tag{25}$$

Based on the above logic relationships, the coordinated switching control is designed via the enabling function H$_D$(P$_i$,T$_j$) and

the inhibitor P$_{reDI}$(P$_i$, T$_j$), and is marked with "▶" as shown in Fig.3, and is implemented as shown in Tables 6 and 7 in the

Appendix.

In Tables 6 and 7, every designed enabling function represents a logic coordinated switching process, whose ultimate aim

are to ensure system security and to reduce operating cost as far as possible. Let us take H$_D$ ($\overline{\overline{P}}$,T$_{17}$) as an example, the descrip-

tion of the enabling function is: when the places P$_{11}$, P$_{16}$ and anyone of P$_7$ and P$_9$ have tokens simultaneously, the discrete tran-

sition T$_{17}$ is triggered. In this case, only if the pre-place P$_{12}$ has token, the operating mode of load will be switched to P$_{13}$. The

logic switching process is explained in detail as: when the MG is assessed as insecure since the VSAI is smaller than the

minimal secure value, while at the same time the FC/MT is running in rate mode, and the battery unit is operating in discharg-

ing mode or in stopping mode because of the lower SOC level, and the MG is providing power supply for all the loads, then the MG needs load-shedding. It is because two renewable energy resource units (WT and PV) cannot regulate their power outputs, and at this moment the FC/MT and battery units have not sufficient dispatchable power, in order to ensure voltage security, the system must execute load-shedding. Other logic switching procedures are similarly explained.

The description in Tables 6 and 7 indicates that when the whole MG is assessed insecure by the VSAI, the corresponding enabling function is activated, so that the connected transition is triggered to coordinately switch the operating mode. The co-ordinated switching control achieves intelligent restructure of operating mode among the agents based on the system security assessment.

4.4 Design of the Switching Control for the Continuous Dynamics Following the Change of Operating Mode

The switching control for continuous dynamics, whose intention is to guarantee the system stability after the operating mode is switched, is also constituted in the local strategy module of the lower level unit agent, and is implemented via the junction function. The switching control presents the following features: (1) it is discrete control driven by discrete event, (2) it is triggered to switch the continuous dynamics when the operating mode changes, and (3) it implements the switching control for continuous dynamics in every agent. The switching control via the junction function $J(T_j, P_{if})$ is marked with "$\cdots\triangleright$" as shown in Fig.3, and is implemented as shown in Table 8 in the Appendix.

The description in Table 8 shows that when the operating mode is switched, the local continuous controller should be also switch to the corresponding operation state so as to rapidly stabilize the system. The switching control achieves intelligent re-structure of local continuous dynamics at the unit agent.

5   Experiment results

In order to test the performance of the proposed control, the simulation test has been done on the MG as shown in Fig.1 on different operation conditions. The event-triggered hybrid control strategies are constructed in decision making module by logic circuits. The battery unit is designed as a grid-forming unit by using droop *f-V* control, while the other DERs are de-signed as grid-followers by using *P-Q* control. The interactive behaviors among the different level of the agents are imple-mented based on the Foundation for Intelligent Physical Agents, Agent Communication Language (FIPA-ACL) in Java Agent Development Framework (JADF). FIPA-ACL messages are characterized by performativity, conversation ID, content and re-ceivers.

Case 1: Load following performance

The total load of the MG from 8.00h to 24.00h during a day is shown in Fig. 4(a), and the wind speed and solar irradiation from 8.00h to 24.00h during the day are given in Fig.4(b) respectively. By using the proposed event-triggered hybrid control, the load following performance of four DER unit agents and voltage performance are obtained as shown in Fig. 4(c) and 4(d)
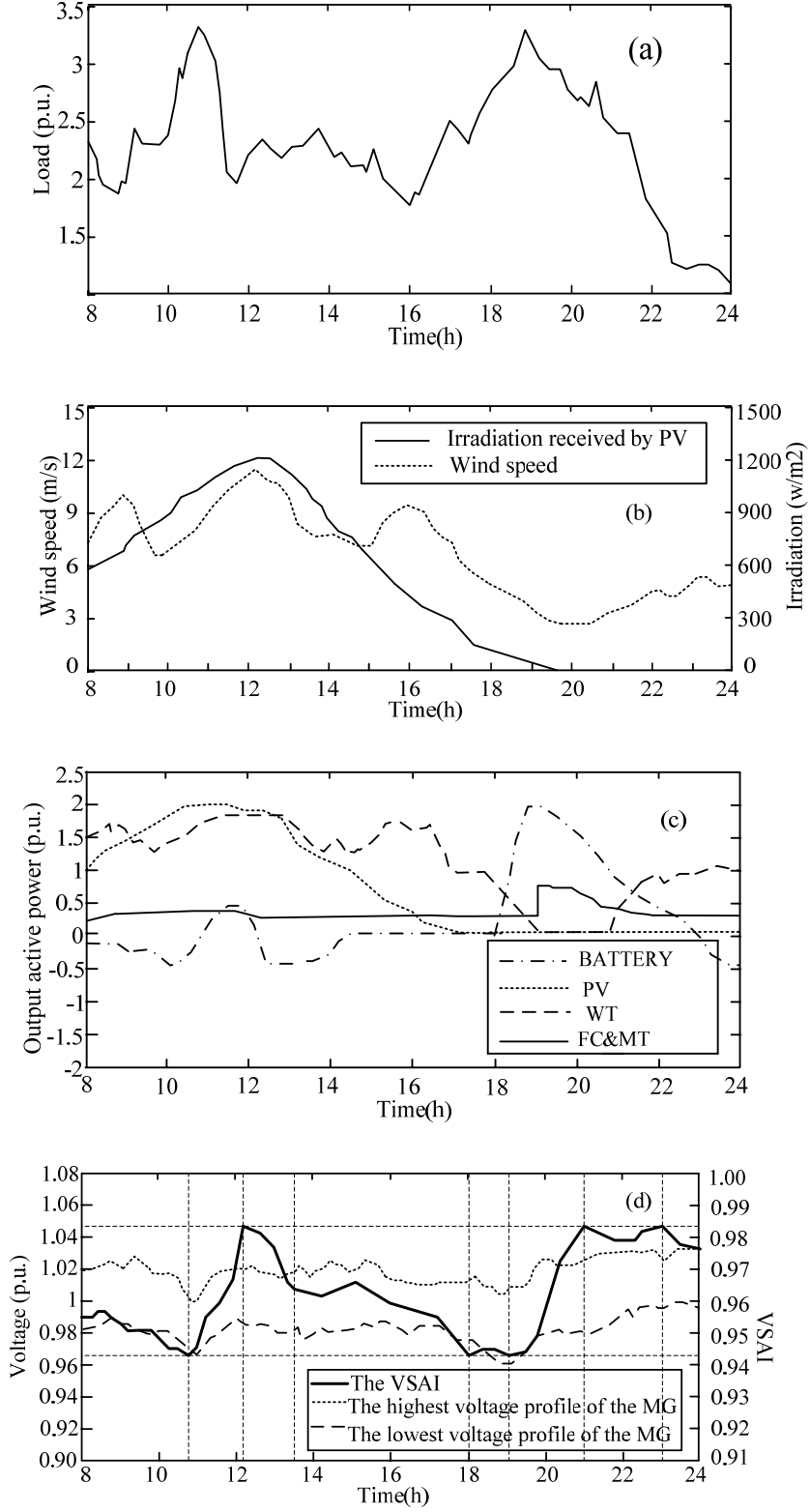
respectively.

Fig.4. Load following performances in the case 1

On the one hand, from Fig.4(c), *it can be seen that in two renewable energy generation unit agents, the switching control for*

their operating mode has been effectively implemented according to the solar irradiation and the wind speed. In detail, the PV

unit agent always operates in MPPT mode from 8.00h to 17.15h because of ample solar irradiation. Only about after 17.15h, the solar irradiation decreases to lower than the threshold value, so that the PV unit agent has to stop operating. It can be also seen that during all the simulation time, triggered by the wind speed, the WT unit agent is switched between three kinds of modes: form about 11.00h to 13.00h, the WT unit is switched to constant output power mode since the wind speed is higher than the higher threshold value; form about 19.00h to 20.45h, it is switched to stopping operating mode since the wind speed is lower than the lower threshold value; and the rest of time, it operates in MPPT mode. On the other hand, from Fig.4(c), *it can be also shown that the coordinated switching control for operating mode has been intelligently implemented among other agents*. In detail, from 8.00h to 10.45h, the power supply from renewable energy generation units is higher than the load demand in the MG, so the battery unit always charges, until the 10.45h instant, the battery unit is switched to discharging mode by the coordinated switching control due to the VSAI drops to the minimum secure value. From 10.45h to 12.15h, the renewable energy generation electricity is lower than the load demand, so the battery unit always discharges, and until the 12.15h instant, the battery unit is switched to charging mode by the coordinated switching control since the VSAI rises to the maximum secure value. The battery unit agent keeps the charging mode until 13.45h. And at the 13.45 instant, the battery unit is switched to stop operating mode and keep this mode until 18.00h, since during this time the renewable energy generation electricity approximately meets the load demand. At the 18.00h instant, the battery unit agent is switched again to discharging mode and maintains the mode until 23.00h. After 23.00h, the battery unit agent is switched again to charging mode. The above shows that, during all simulation time, the battery unit agent is frequently switches between three kinds of modes by the coordinated switching control. Since as a dispatchable unit, the battery unit agent here acts as master source implementing a grid-forming control to maintain the security of system. As a creative idea, here use the constraint condition of the VSAI to trigger the coordinated switching control. As a result, the operating mode of the battery unit agent can be intelligently switched so as to maintain power balance and ensure voltage security. It can be also seen that, during most of the simulation time, the battery unit agent has sufficient dispatchable power so that the FC/MT unit agent must operate in low power output mode to reduce the operating cost as far as possible. Only during 19.00h to 20.50h, the battery unit agent has not sufficient capability to match larger unbalanced power, while the FC/MT unit agent is switched to the rated operating mode by the coordinated switching control to increase the power supply. In addition, from Fig.4(c), *it also implies that the switching control for the continuous dynamics in every DER unit agent is effective, since after the operating mode of every unit agent is switched, their output power can be effectively regulated in new operating mode.* Fig.4(d) displays the highest and lowest voltage profiles of the MG and the VSAI. On this experiment study, according to the criterion of information fusion technique, the maximum and minimum secure values of the VSAI are set as 0.943 and 0.983 respectively. In Fig.4(d), it shows that the VSAI is always limited within the secure range of [0.943, 0.983], and in case the VSAI drops (or rises) to the minimum secure value (or maximum secure value), the coordinated switching control is triggered to switch operating mode. It can be also seen that during all the simulation time, the voltage is controlled within the secure range from 0.94p.u. to 1.04p.u., and the fluctuation value is limited

in the range of ± 4 percentage of rating value.

In this case, the messages exchanged between agents are shown in Fig.5. Due to the coordinated control agent (CCA) is mainly responsible for coordinating and managing the operating modes of all DER units, thus the PV and WT unit agents need "INFORM" their operating mode to the CCA when they are switched by the internal switching control such as at 11.00h, 13.00h, 17.45h, 19.00h, and 20.45h, respectively. In addition, when the VSAI rises (or drops) to maximum (or minimum) secure value, the CCA sends "REQUEST" message to corresponding unit agent like the battery unit agent and FC/MT unit agent according to the designed coordinated switching control strategies, at the moment, if the unit agent returns "AGREE" messages to the CCA, then the coordinated switching control is implemented such as at 10.45h, 12.15h, 13.45h, 18.00h, 19.00h, 20.50h and 23.00h, respectively.

From the above experimental results, it implies that the interactive coordination among agents can be timely implemented based on the intelligent MAS platform, so that the operating mode of the MG can be intelligently restructured according to the change of operation situation by the proposed event-triggered hybrid control to ensure the security of voltage and the stability after mode switching, as well to reduce operating cost as far as possible.
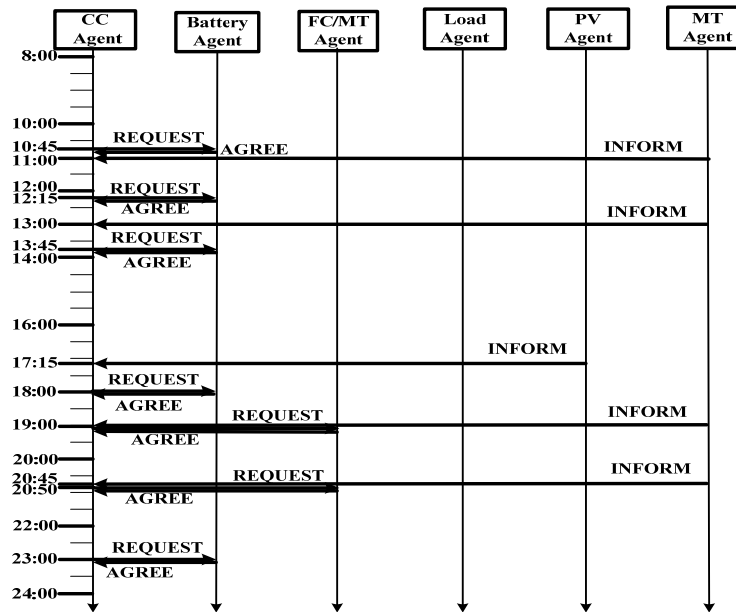

Fig.5. Messages exchanged between agents based on MAS platform

Case 2: Performance under non-planned islanding operation

It is well known that a MG can operate in both grid-connected and islanded modes. An unplanned disconnection from the main grid is usually regarded as a very severe example of islanding. The purpose of case 2 is to investigate the control performances under this case. The non-planned islanding is detected to occur at $t = 10h$.

The total load of the MG from 8.00h to 24.00h during a day is shown in Fig. 6(a), and the wind speed and solar irradiation from 8.00h to 24.00h during the day is same as Fig.4(b). Figs. 6(b) and 6(c) show the active power outputs of the four DER unit agents and voltage responses respectively on the non-planned islanding situation. In grid-connected mode, the load de-

mand is mainly met by the main grid, and all DERs operate in grid-following mode. But in islanded mode, by the MAS based event-triggered hybrid control, all DERs can be effectively grouped together and depend on each other to supply the required energy and to maintain the voltages of MG. In detail, at the islanding instant, in order to meet load demand, the battery unit agent is immediately switched to discharging mode from charging mode, but the mode switching has a small time delay, which leads to a sharp decline of voltage to 0.91p.u. Soon after, the voltages return to the normal range. At the islanded instant, due to sufficient solar and wind energy, both renewable energy generation units operate in MPPT mode, and grouped together with the battery unit, they are able to meet the load demand. Therefore the FC&MT unit is still in low output power mode with just a small output power regulation. After the islanding instant, due to the difference of load curve, compared with the case 1, the operating modes of DERs in case 2 are also very different, such as during 18.00h to 20.25h, even when both renewable energy resource units stop operating, only one battery unit is still able to satisfy the load demand, thus during all the simulation time, the FC&MT unit is always in low output power mode to reduce operating cost as far as possible. In case 2, except for the islanding instant, the VSAI is limited within the secure range, and the voltages are maintained in the secure range of 0.97p.u. to 1.03p.u.. From the experimental results of Figs.6(b) and 6(c), it also implies that the proposed event-triggered hybrid control can ensure the security of voltage and the stability after large disturbance, as well to reduce operating cost as far as possible through effective restructure of operating mode according to variable operation condition.
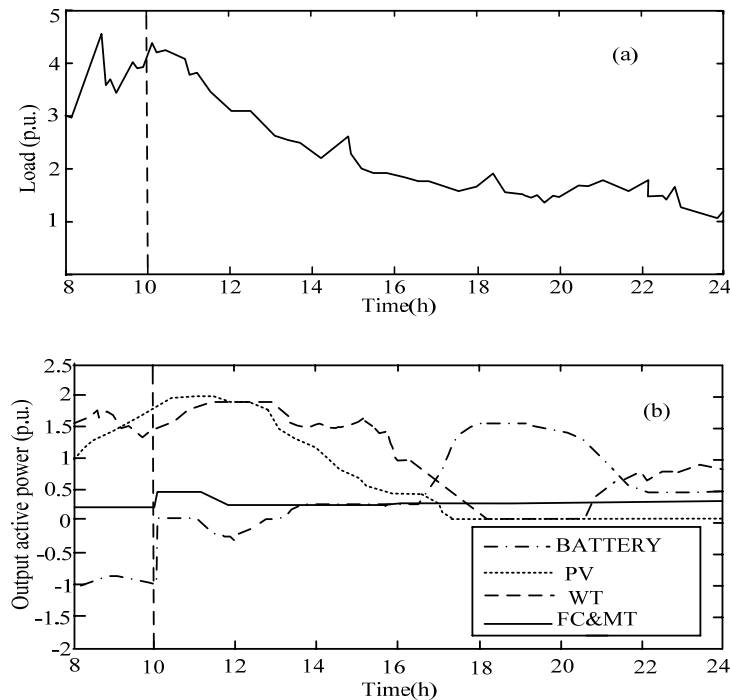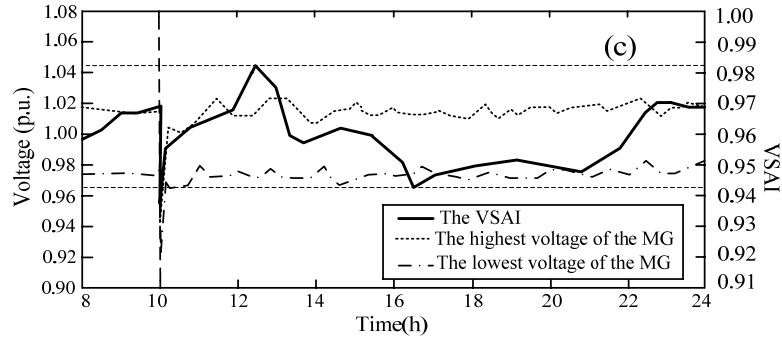
Fig.6. Control performance under an islanding disturbance in case 2

6   Conclusion

In this paper, a MAS based event-triggered hybrid control including three kinds of switching controls is researched for the energy supply more secure and high-efficient. As original works, the three kinds of switching controls are respectively constructed based on the DHPN models by designing multiple enabling functions that can be activated by different triggering conditions such as the constraint conditions of continuous state or the occurrences of discrete events. Moreover, the interactive coordination among the three kinds of switching controls is implemented based on the intelligent MAS platform, so that the operating mode of the MG can be intelligently restructured according to the change of operation situation. Simulation results show that the smart hybrid control strategies can ensure MG to effectively use distributed energy resources to meet variable load demand with high reliability, flexibility and efficiency.

Acknowledgment

Appendix

Table 1. Description of the discrete places in the DHPN model

Discrete Places	Description
P_1	Maximum Power Point Tracking (MPPT) operating mode in the Wind Turbine (WT) unit agent
P_2	Stopping operating mode in the WT unit agent
P_3	Constant power output operating mode in the WT unit agent
P_4	MPPT operating mode in the Photovoltaic (PV) unit agent
P_5	Stopping operating mode in the PV unit agent
P_6	Charging operating mode in the battery unit agent
P_7	Discharging operating mode in the battery unit agent
P_8	Stopping operating mode with maximal State of Charge (SOC) in the battery unit agent
P_9	Stopping operating mode with minimal SOC in the battery unit

P$_{10}$		Low power output mode in the Fuel Cell/Microturbine (FC/MT) unit agent
P$_{11}$		Rated power output mode in FC/MT unit agent
P$_{12}$		Full load operating mode in the load unit agent
P$_{13}$		Part load operating mode in the load unit agent
P$_{14}$		light load operating mode in the load unit agent
P$_{15}$		Normal voltage operating mode in the MG
P$_{16}$		Insecure low voltage operating mode in the MG
P$_{17}$		Insecure high voltage operating mode in the MG

Table 2. Description of the discrete transitions in the DHPN model

Discrete Transitions	Description
T$_1$	The WT unit switches to stopping mode from MPPT mode
T$_2$	The WT unit switches to MPPT mode from stopping mode
T$_3$	The WT unit switches to constant output mode from MPPT mode
T$_4$	The WT unit switches to MPPT mode from constant output mode
T$_5$	The WT switches to stopping mode from constant output mode
T$_6$	The WT switches to constant output mode from stopping mode
T$_7$	The PV switches to stopping mode from MPPT mode
T$_8$	The PV switches to MPPT mode from stopping mode
T$_9$	The battery switches to discharging mode from charging mode
T$_{10}$	The battery switches to discharging mode from stopping mode with maximal SOC
T$_{11}$	The battery switches to charging mode from discharging mode
T$_{12}$	The battery switches to charging mode from stopping mode with minimal SOC
T$_{13}$	The battery stops discharging because SOC reaches to minimal value
T$_{14}$	The battery stops charging because SOC reaches to maximal value
T$_{15}$	The FC/MT switches to rated mode from low output mode
T$_{16}$	The FC/MT switches to low output mode from rated mode
T$_{17}$	The part load shedding
T$_{18}$	The maximal load shedding
T$_{19}$	The load partly restored
T$_{20}$	The load fully restored
T$_{21}$	The VSAI is smaller than minimal secure value
T$_{22}$	The VSAI is larger than maximal secure value
T$_{23}$	The VSAI rises into normal range
T$_{24}$	The VSAI drops into normal range

Table 3. Description of differential places in the DHPN model

Differential Places	Description
P1f- P5f	Continuous states corresponding to the WT, PV, battery, FC/MT unit agent respectively
P6f	Bus voltage states in the MG

Table 4. Description of differential transitions

Differential Transitions	Description
T1f and T2f	Continuous dynamics of the WT unit in P1 and P3 operating modes respectively
T3f	Continuous dynamics of the PV unit in P4 operating mode
T4f and T5f	Continuous dynamics of the battery unit in P6 and P7 operating modes respectively
T6f	Continuous dynamics of the FC/MT unit in P10 operating mode
T7f-- T9f	Continuous dynamics of the load unit in P13, P14 and P12 operating modes respectively
T10f-- T12f	Real-timely dynamic voltages of the MG in P15---P17 operating modes respectively

Table 5. Implementing of the switching control for operating mode in unit agent through the designed enabling functions

Functions	Description
HDF (P1f,T1)	When the continuous state variable drops to $\nu \leq \nu_{ci}$, the enabling function HDF (P1f,T1) is activated so that discrete transition T1 is triggered and the operating mode of WT agent is switched to P2 that $P_w = 0$.
HDF (P1f,T2)	When the continuous state variable rises to $\nu_{ci} < \nu \leq \nu_R$, the enabling function HDF (P1f,T2) is activated so that discrete transition T2 is triggered and the operating mode of WT agent is switched to P1 that $P_w = P_R(\nu - \nu_{ci})/(\nu_R - \nu_{ci})$.
HDF (P1f,T3)	When the continuous state variable rises to $\nu_R < \nu \leq \nu_{co}$, the enabling function HDF (P1f,T3) is activated so that discrete transition T3 is triggered and the operating mode of WT agent is switched to P3 that $P_w = P_R$.
HDF (P1f,T5)	When the continuous state variable rises to $\nu > \nu_{co}$, the enabling function HDF (P1f,T5) is activated so that discrete transition T5 is triggered, and the operating mode of WT agent is switched to P2 that $P_w = 0$.
HDF (P1f,T6)	When the continuous state variable drops to $\nu_R < \nu \leq \nu_{co}$, the enabling function HDF (P1f,T6) is activated so that discrete transition T6 is triggered and the operating mode of WT agent is switched to P3 that $P_w = P_R$.
HDF (P1f,T4)	When the continuous state variable drops to $\nu_{ci} < \nu \leq \nu_R$, the enabling function HDF (P1f,T4) is activated so that discrete transition T4 is triggered and the operating mode of WT agent is switched to P1 that $P_w = P_R(\nu - \nu_{ci})/(\nu_R - \nu_{ci})$.
HDF (P2f,T7)	When the continuous state variable drops to $G_{ing} \leq C$, the enabling function HDF (P2f,T7) is activated so that discrete transition T7 is triggered and the operating mode of PV agent is switched to P5 that $P_{PV} = 0$.
HDF (P2f,T8)	When the continuous state variable rises to $G_{ing} > C$, the enabling function HDF (P2f,T8) is activated so that discrete transition T8 is triggered and the operating mode of PV agent is switched to P4 that $P_{PV} = P_{stc} G_{ing} \left(1 + k(T_c - T_r)\right)/G_{stc}$.
HDF (P3f,T13)	When the continuous state variable drops to SOC=SOCmin, the enabling function HDF (P3f,T13) is activated so that discrete transition

	T13 is triggered and the operating mode of battery agent is switched to P9 that $P_- = 0$.
$H_{DF}(P3f,T14)$	When the continuous state variable rises to SOC=SOCmax, the enabling function H_{DF} (P3f,T14) is activated so that discrete transition T14 is triggered and the operating mode of battery agent is switched to P8 that $P_+ = 0$.
$H_{DF}(P6f,T21)$	When the continuous voltage assessment index drops to $m(U) \leq U_{min}$, the enabling function H_{DF} (P6f,T21) is activated so that discrete transition T21 is triggered and the operating mode of coordinated agent is switched to P16.
$H_{DF}(P6f,T23)$	When the continuous voltage assessment index rises to $U_{min} < m(U) \leq U_e$, the enabling function H_{DF} (P6f,T23) is activated so that T23 is triggered and the operating mode of coordinated agent is switched to P15.
$H_{DF}(P6f,T22)$	When the continuous voltage assessment index rises to $m(U) \geq U_{max}$, the enabling function H_{DF} (P6f,T22) is activated so that T22 is triggered and the operating mode of coordinated agent is switched to P17.
H_{DF} (P6f,T24)	When the continuous voltage assessment index drops to $U_e < m(U) < U_{max}$, the enabling function H_{DF} (P6f,T24) is activated so that T24 is triggered and the operating mode of coordinated agent is switched to P15.

Table 6. Implementing of the coordinated switching control for operating mode among agents through the designed enabling functions

Functions	Description
H_D (P16,T9)	When the discrete pre-place P16 has token, the enabling function is activated so that discrete transition T9 is triggered. In this case, only if the pre-place P6 has token, the operating mode of battery will be switched to P7.
H_D (P16,T10)	When the discrete pre-place P16 has token, the discrete transition T10 is also triggered. In this case, only if P8 has token, the operating mode of battery will be switched to P7.
$H_D(\overline{P},T15)$	When the place P16 and anyone of P7 and P9 have tokens simultaneously, the discrete transition T15 is triggered. In this case, only if the pre-place P10 has token, the operating mode of FC/MT will be switched to P11.
H_D ($\overline{\overline{P}}$,T17)	When the places P11, P16 and anyone of P7 and P9 have tokens simultaneously, the discrete transition T17 is triggered. In this case, only if the pre-place P12 has token, the operating mode of load will be switched to P13.
$H_D(\overline{\overline{P}},T18)$	When the places P11, P16 and anyone of P7 and P9 have tokens simultaneously, the discrete transition T18 is also triggered. In this case, only if the pre-place P13 has token, the operating mode of load will be switched to P14.
H_D (P17,T19)	When the discrete pre-place P17 has token, the discrete transition T19 is triggered. In this case, only if the pre-place P14 has token, the operating mode of load will be switched to P13.
H_D (P17,T20)	When the discrete pre-place P17 has token, the discrete transition T20 is also triggered. In this case, only if P13 has token, the operating mode of load will be switched to P12.
$H_D(\tilde{P},T16)$	When the places P12 and P17 have tokens simultaneously, the discrete transition T16 is triggered. In this case, only if P11 has token, the operating mode of FC/MT will be switched to P10.
H_D ($\tilde{\tilde{P}}$,T11)	When the places P10, P12 and P17 have tokens simultaneously, T11 is triggered. In this case, only if P7 has token, the operating mode of battery will be switched to P6.
H_D ($\hat{P}$,T12)	When the places P10, P12, P17 and anyone of P6 and P8 have tokens simultaneously, the discrete transition T12 is triggered. In this case, only if the pre-place P4 has token, the operating mode of PV will be switched to P5.

Table 7. Restricting of the switching control for operating mode via the designed inhibitor functions

Functions	Description
PreDI($\tilde{\tilde{P}}$,T2)	The discrete transition T2 is restricted not triggering when the places P10, P12 and P17 have token simultaneously.
PreDI($\tilde{\tilde{P}}$,T6)	The discrete transition T6 is restricted not triggering when the places P10, P12 and P17 have token simultaneously.
PreDI($\tilde{\tilde{P}}$,T8)	The discrete transition T2 is restricted not triggering when the places P10, P12 and P17 have marking simultaneously.

Table 8. Implementing of the switching control for continuous dynamics via the designed junction function

Functions	Description
J(T3,P1f)	When the discrete transition T3 fires, the continuous controller for P1f dynamics is switched to the constant power mode from the MPPT mode.
J(T4,P1f)	When the discrete transition T4 fires, the continuous controller for P1f dynamics is switched to the MPPT mode from the constant power mode.
J(T9,P3f) J(T10,P3f)	When the discrete transition T9 or T10 fires, the continuous controller for P3f dynamics is switched to the discharging mode from the charging mode.
J(T11,P3f) J(T12,P3f)	When the discrete transition T11 or T12 fires, the continuous controller for P3f dynamics is switched to the charging mode from the discharging mode.
J(T17,P5f)	When the discrete transition T17 fires, the continuous controller for P5f dynamics is switched to the part load shedding mode from the full load mode.
J(T18,P5f)	When the discrete transition T18 fires, the continuous controller for P5f dynamics is switched to the light load mode from the part load mode.
J(T19,P5f)	When the discrete transition T19 fires, the continuous controller for P5f dynamics is switched to the part load mode from the light load mode.
J(T20,P5f)	When the discrete transition T20 fires, the continuous controller for P5f dynamics is switched to the part load mode from the full load mode.

References

[1] R. H. Lassetter, A. Akhil, et al, "The CERTS Microgrid concept," http://certs.lb.lgov/pdf/50829.pdf.

[2] N. Hatziargyriou, H. Asano, et al, "Microgrids," IEEE Power & Energy Magazine, vol.6, pp.78-94, 2007.

[3] R. H. Lasseter, "Microgrids," Power Engineering Society Winter Meeting, New York, UAS, 2002.

[4] R. H. Lasseter, P. Piagi, "Control and design of microgrid components, final project report," http://www.pserc.org.

[5] IEEE Std.1547.4-2007, "Island systems with electric power systems," 2007.

[6] M. Satoshi, "Montreal 2006 symposium on Micrigrids: overview of Micrigrid research and development activities in Japan," http://der.lbl.gov/new_site/DER.htm.

[7] M. Sanchez, "Montreal 2006 symposium on Micrigrids: overview of micrigrid research and development activities in the EU," http://der.lbl.gov/new_site/DER.htm.

[8] Josep M. Guerrero, P. C. Loh, M. Chandorkar, T. L. Lee, "Advanced control architectures for intelligent Microgrids – Part I: decentralized and hierarchical control," IEEE Transactions on Industrial Electronics, vol.60, pp. 1254-1262, 2012.

[9] A. R. Yasser, E. S. F. Ehab, "Adaptive decentralized droop controller to preserve power sharing stability of paralleled inverters in distributed generation microgrids," IEEE Transactions on Power Electronics, vol.23, pp. 2806-2816, 2008.

[10] E. Barklund, N. Pogaku, M. Prodanovic, C. H. Aramburo, T. C. Green, "Energy management in autonomous Microgrid using stability –constrained droop control of inverter," IEEE Transactions on Power Electronics, vol.25, pp.2346-2352, 2008.

[11] Z. H. Jiang, L. J. Gao, R. A. Dougal, "Flexible multi-objective control of power converter in active hybrid fuel cell/ battery power sources," IEEE Tran. Power Electr,vol.20, pp.245-254, 2005.

[12] Z. H. Jiang, L..J. Gao, R. A. Dougal, "Adaptive control strategy for active power sharing in hybrid fuel cell/battery power sources," IEEE Tran. Energy Conver, vol.22, pp.183-194, 2007.

[13] D. B. Nelson, M. N. Nehrir, C. Wang, "Unit sizing and cost analysis of stand-alone hybrid wind/PV/ fuel cell power generation system," Renewable Energy, vol.31, pp.1641-1656, 2006.

[14] L..J. Gao, Z. H. Jiang, R. A. Dougal, "An actively controlled fuel cell/battery hybrid to meet pulsed power demands," Journal Power Sources, vol.130, pp.202-207, 2004.

[15] S. Ashok, "Optimised model for community-based hybrid energy system," Renewable Energy, vol.32, pp.1155-1164, 2002.

[16] S. D. J. Mcarthur, E. M. Davidson, V. M. Catterson, et al, "Multiagent systems for power engineering applications, Part I: Concepts, approaches, and technical challenges," IEEE Transactions on Power Systems, vol.22, pp.1743-1752, 2007.

[17] C. C. Liu, "Agent modeling for integrated power systems," Final Project Report, Power Systems Engineering Research Center, PSERC, September, 2008.

[18] A. L. Dimeas, N. D. Hatziargyrious, "Agent based control for Microgrids," IEEE PES General Meeting, Tampa, FL, June, 2007.

[19] A. L. Dimeas, N. D. Hatziargyrious, "Operation of a multi-agent system for Microgrid control," IEEE Transactions on Power Systems, vol.20, pp.1447-1455, 2005.

[20] C. X. Dou, B. Liu, "Hierarchical hybrid control for improving comprehensive performance in smart power system," International Journal of Electrical Power & Energy Systems, vol.43, pp.595-606, 2012.

[21] C. X. Dou, B. Liu, "Transient control for Microgrid with multiple distributed generations based on hybrid system theory," International Journal of Electrical Power & Energy Systems, vol.42, pp.408-417, 2012.

[22] C. X. Dou, D. L. Liu, X. B. Jia, F. Zhao, "Management and control for smart microgrid based on hybrid control theory," Electric Power Component and System, vol.39, pp.813-32, 2011.

[23] V. K. Paruchuri, A. Davari, A. Feliachi, "Hybrid modeling of power system using hybrid Petri net," In Proc. Southeastern Symposium on System Theory, pp.221-224, 2005.

[24] N. Lu, J. H. Chow, A. A. Desrochers, "A multi-layer Petri net model for deregulated electric power systems," In Proc. Amer. Contr. Conf., Anchorage, AK, pp. 513-518, 2002.

[25] J. Sun, S. Y. Qin, Y. H. Song, "Fault diagnosis of electric power systems based on fuzzy Petri nets," IEEE Transactions on Power System, vol.19, pp.2053-2059, 2004.

[26] K. Seethalekshmi, S. N. Singh, S. C. Srivastava, "A synchrophasor assisted frequency and voltage stability based load shedding scheme for self-healing of power system," IEEE Trans. Smart Grid, vol. 2, pp. 221-230, 2011.

[27] S. Mohammad, A. A. W. Mohammad, C. Oksam, "A reliable skin detection using Dempster-Shafer theory of evidence," International Conference on Computational Science and Its Applications, vol.5593, pp.764-779, 2009.